(2)

SEMICONDUCTOR ALLOY ENGINEERING FOR HIGH-SPEED DEVICES

Final Report

August 1988

By: A. Sher, Associate Director
S. Krishnamurthy, Research Physicist
Physical Electronics Laboratory

A.-B. Chen
Auburn University

Prepared for:

United States Air Force
Air Force Systems Command
Air Force Office of Scientific Research
Building 410
Bolling Air Force Base, D.C. 20332-6448

Sponsored by Advanced Research Projects Agency (DoD)
ARPA Order 5396
Monitored by Captain Kevin Malloy
under Contract F49620-85-C-0103

SRI Project 8725

SRI International
333 Ravenswood Avenue
Menlo Park, California 94025-3493
(415) 326-6200
Telex: 334486

UNCLASSIFIED

SECURITY CLASSIFICATION OF THIS PAGE

ADA200356

REPORT DOCUMENTATION PAGE

Form Approved OMB No. 0704-0188

1a. REPORT SECURITY CLASSIFICATION UNCLASSIFIED	1b. RESTRICTIVE MARKINGS
2a. SECURITY CLASSIFICATION AUTHORITY	3. DISTRIBUTION/AVAILABILITY OF REPORT Approved for public release; distribution unlimited.
2b. DECLASSIFICATION/DOWNGRADING SCHEDULE	
4. PERFORMING ORGANIZATION REPORT NUMBER(S) Final Report SRI Project 8725	5. MONITORING ORGANIZATION REPORT NUMBER(S) AFOSR-TR- 88-0981
6a. NAME OF PERFORMING ORGANIZATION SRI International 6b. OFFICE SYMBOL (If applicable)	7a. NAME OF MONITORING ORGANIZATION Air Force Office of Scientific Research
6c. ADDRESS (City, State, and ZIP Code) 333 Ravenswood Avenue Menlo Park, California 94025	7b. ADDRESS (City, State, and ZIP Code) Building 410 Bolling AFB, D.C. 20332-6448
8a. NAME OF FUNDING/SPONSORING ORGANIZATION AFOSR 8b. OFFICE SYMBOL (If applicable) NE	9. PROCUREMENT INSTRUMENT IDENTIFICATION NUMBER F49620-85-C-0103
8c. ADDRESS (City, State, and ZIP Code) Bldg 410 Bolling AFB, DC 20332	10. SOURCE OF FUNDING NUMBERS PROGRAM ELEMENT NO. 61102F; PROJECT NO. 2306; TASK NO B1; WORK UNIT ACCESSION NO.
11. TITLE (Include Security Classification) Semiconductor Alloy Engineering for High-Speed Devices	
12. PERSONAL AUTHOR(S) A. Sher and S. Krishnamurthy	
13a. TYPE OF REPORT Final 13b. TIME COVERED FROM Jun 85 TO Aug 88	14. DATE OF REPORT (Year, Month, Day) 1988 August 15. PAGE COUNT 27
16. SUPPLEMENTARY NOTATION ARPA Order 5396	
17. COSATI CODES FIELD / GROUP / SUB-GROUP	18. SUBJECT TERMS (Continue on reverse if necessary and identify by block number) Semiconductors Scattering Mechanisms

19. ABSTRACT (Continue on reverse if necessary and identify by block number)

Realistic band structures of III-V compounds and alloys are used in the studies of ballistic and high field drift transport. The effect of scattering mechanisms such as ionized impurity, polar optic phonon, alloy disorder, deformation potential coupled intervalley scattering, and electron-electron scattering on electron mean free path and velocity-field characteristics are studied. *Ab initio* calculation of the coupling constants necessary to evaluate these scattering rates are made. The hot electron transistor characteristics calculated with no adjustable parameter agrees very well with experimental values. The efficiency of ballistic devices are evaluated using the calculated velocity mean free path. We conclude that for ballistic devices with thicker base width (≈500 Å) GaInAs alloys are preferred to GaAs. However, for devices with very small base width (≈100 Å) no material is appreciably better than GaAs. In the studies of drift transport, we had initially used the electron temperature model to obtain the v-E curves for various semiconductor compounds and alloys. These model calculations were useful to obtain the trends. The steady-state Boltzmann transport equation must be solved without such limiting approximations to obtain quantitatively more accurate v-E curves. Toward that end, we have developed an eigenvalue method that is two to three orders of magnitude faster than the existing numerical methods. Using the eigenvalue method, the v-E curves in various semiconductors and alloys are obtained for E < 15 kV/cm. From the calculated values of peak velocity, threshold field, and pair-production energy, we conclude that high-speed devices made of $Ga_{0.47}In_{0.53}As$, $InP_{0.75}As_{0.25}$, and $InP_{0.75}Sb_{0.25}$ will be more efficient than devices made from GaAs.

20. DISTRIBUTION/AVAILABILITY OF ABSTRACT ☐ UNCLASSIFIED/UNLIMITED ☐ SAME AS RPT. ☐ OTIC USERS	21. ABSTRACT SECURITY CLASSIFICATION UNCLASSIFIED
22a. NAME OF RESPONSIBLE INDIVIDUAL Malloy	22b. TELEPHONE (Include Area Code) (202) 767-4931 22c. OFFICE SYMBOL NE

DD Form 1473, JUN 86 Previous editions are obsolete. SECURITY CLASSIFICATION OF THIS PAGE

SRI International

SEMICONDUCTOR ALLOY ENGINEERING FOR HIGH-SPEED DEVICES

Final Report

August 1988

By: A. Sher, Associate Director
S. Krishnamurthy, Research Physicist
Physical Electronics Laboratory

A.-B. Chen
Auburn University

Prepared for:

United States Air Force
Air Force Systems Command
Air Force Office of Scientific Research
Building 410
Bolling Air Force Base, D.C. 20332-6448

Sponsored by Advanced Research Projects Agency (DoD)
ARPA Order 5396
Monitored by Captain Kevin Malloy
under Contract F49620-85-C-0103

SRI Project 8725

Approved:

Ivor Brodie, Director
Physical Electronics Laboratory

W.F. Greenman, Vice President
Advanced Technology Division

SRI International

CONTENTS

ILLUSTRATIONS

TABLE

I INTRODUCTION

A. Background

In the last ten years, high-speed (10- to 100-GHz) devices have been tested in myriad operating modes and geometries. The goal of these efforts have been to develop efficient discrete elements that can be readily fabricated into reliable systems with high production yield. While the tried and true silicon semiconductor continues to be the workhorse of the industry, its relatively high effective mass begins, makes it less attractive that some of the III-V compounds (e.g., GaAs, InP, and certain alloys) once design frequencies are high.

Moreover, many of the new device designs call for heterojunctions (e.g., tunneling junctions in hot electron transistors), high mobility channels (e.g., quantum well structures) and other special characteristics. The question of optimum materials selection for these multimaterial structures is nontrivial. The advent of such growth methods as molecular beam epitaxy (MBE) and metal organic chemical vapor deposition (MOCVD) have made it possible to prepare multilayer thin films of different materials for each different part of a device (e.g., the emitter, collector, and base of a transistor). There are general guidelines within which materials are compatible. Most of the semiconductors of interest fall into the diamond or zincblende crystal structure groups, which can be grown compatibly on dissimilar substrates without device-degrading defects provided that the lattice constants of the substrate and epitaxial layers are not too different.

In this report, we address only a subset of questions bearing on materials selection; however, these questions are central to high-speed performance. The major question is, which materials offer the best set of performance-limiting parameters for the device's active transport region (usually the base)? The number of possible materials from which to select is enormous: the compounds and alloys made from the cations, aluminum, gallium, indium, and the anions phosphorous, arsenic, and antimony. Thus, predictions of an accurate theory can serve to reduce greatly the number of experiments needed to optimize performance.

B. Device Operating Modes

The answer to our question differs for devices intended to function in grossly different operating modes. The modes can be separated into three general classes: drift, ballistic, and tunneling. The distinction between the classes is determined by the length of the active region of the device.

- If the device is long compared to the majority carrier velocity mean free path, then it functions in the *drift mode*, in which carriers make many collisions as they transport across the device. The mean free path reduces to the momentum mean free path only if the effective mass is a constant for all the populated states. Generally, the lower size limit for the drift mode is a few tenths of a micrometer.

- *Ballistic mode* devices are those whose scale size falls between the velocity mean free path, and the tunneling thickness, generally tens of angstroms.
- The *tunneling mode* devices are the smallest ones.

Ballistic mode devices have most of the carriers transport through the active region with few or no collisions. Most of this report is devoted to materials choices for ballistic mode devices, and nothing more will be said about the tunneling modes.

The differing criteria for materials choices in the drift and ballistic modes lead to distinct optimum choices.

- All of the drift mode device performance-limiting-parameters can be expressed in terms of features of the drift velocity-field curves: At low fields, these curves increase linearly with field (the slope is the low field mobility). For some materials (e.g., silicon and other indirect bandgap semiconductors), these curves then saturate; in others (GaAs, InP, and most direct-bandgap semiconductors), they first reach a peak, then saturate after descending through a valley.
- The ballistic mode places a premium on the speed with which the carrier moves, and the fraction of electrons reaching the collector without colliding. The speed and device dimensions determine the upper cutoff frequency and the ballistic fraction is related to efficiency.

C. Significance of Band Structure

A reliable prediction of the device-performance-limiting parameters of high-electron-dominated high-speed structures requires the use of accurate band structures, rather than effective-mass approximations. This is because the carriers occupy highly excited states in which the curvature of the bands ε_k changes rapidly with crystal momentum k. This affects not only the effective mass, but also the group velocity and the density of states.

The density of states is particularly important in calculating scattering rate. It has been traditional to calculate scattering rates from effective-mass approximations. Coupling constants for some scattering mechanisms (e.g., electron to polar optical phonons) are reliably calculated, while others (notably electron to deformation-potential-coupled longitudinal acoustic phonons) are not. [We here restrict our discussions to electrons, although some light-hole band devices have been suggested.] Hence, it is common practice to use effective-mass band structures for the central Γ-valley and satellite L-valley when calculating the polar phonon impurity and electron-electron contributions to intervalley scattering, then to choose the deformation potential coupling constant such that the net scattering rate fits an experiment (e.g., four-wave optical mixing). The use of effective-mass band structures, which produce densities of final states that are too small, results in underestimates of polar phonon and the impurity scattering. As a consequence, the deformation potential coupling constant needed to fit experimental data is larger than its true value. This procedure distorts the relative importance of the deformation potential and other mechanisms. When the various mechanisms are applied to situations differing from those of the experimental data to which they were fit, this procedure can introduce serious errors. Thus, accurate band structures are required to make reliable predictions about hot electron transport in any of the operating modes.

It is also desirable to calculate all the coupling constants so as to eliminate the need for direct-scattering-related experimental information. The electron-scattering mechanisms we have treated this way are longitudinal and transverse for both optical and acoustic phonons, screened charged impurity, plasma, and alloy. Alloy band structures and scattering rates are calculated together in the coherent potential approximation (CPA) formalism.

D. Organization of the Report

Section II summarizes calculation of scattering rates resulting from various scattering mechanisms. We discuss our choice of materials for ballistic transport in Section III and that for drift transport in Section IV. Because most of the results have appeared in the form of journal publication, the details are not given. Conclusions are given in Section V. A Bibliography of journal publications and conference papers resulting from this 36-month research follows the list of references.

II CALCULATION OF SCATTERING RATES FROM VARIOUS MECHANISMS

The full band structure is used in the calculation of scattering rates resulting from ionized impurity, longitudinal optic (LO) phonons, deformation-potential-coupled intervalley scattering, electron-electron scattering. and (in the case of alloys) disorder scattering. The inclusion of full band structure makes the Brillouin zone (BZ) sum more time-consuming, because the sum must be carried out over the entire BZ, instead of the usual 1/48th of BZ. All coupling constants necessary to evaluate the scattering rates are obtained from the underlying band structure. Because some of these results have been described in the quarterly reports, the procedure is discussed here in brief. Details can be obtained from our published papers.

Our tight-binding (TB) Hamiltonian $H_0(k)$ includes all long-range interactions (Krishnamurthy, Sher, and Chen, 1986). Our basis contains the Gaussian orbitals of the type $|\alpha lj\rangle$ (α can be s, p_x, p_y, or p_z) for each sublattice, j, and each cell, l. The Bloch orbitals $|\alpha\vec{k}j\rangle$ are expanded in terms of large number of plane waves $|\vec{k}+\vec{G}\rangle$ ($\vec{G}$ is reciprocal lattice vector) and the $H_0(\vec{k})$ is obtained by using pseudopotentials. The band structure is fine-tuned to experimental values by adding an adjustable Hamiltonian $H_1(\vec{k})$. The expansion coefficients $A_{\alpha j}$, which are eigenvectors of $H_0(\vec{k}) + H_1(\vec{k})$, are used to obtain the wave function required in the calculation of various scattering rate.

A. Ionized Impurities

The potential for ionized impurities scattering is given by:

$$V_{ei} = \left[\frac{4\pi e^2}{\kappa_\infty V}\right] \sum_{\vec{q}} e^{i\vec{q}\cdot\vec{r}} (q^2 + \lambda^2)^{-1}$$

where

$$\lambda = [(4\pi\, n_I\, e^2)/(\kappa_\infty k_B T)]^{1/2} \quad ,$$

and n_I is the impurity density, N_I/V, κ_∞ is the infinite frequency dielectric constant, k_B is Boltzmann's constant, e is the electron charge, and T is the lattice temperature in Kelvins. For scattering from $\vec{k}'$ to $\vec{k}$,

$$S_{imp}(\vec{k},\vec{k'}) = \frac{2\pi}{\hbar} \, |\langle \vec{k}|V_{ei}|\vec{k'}\rangle|^2 \, \delta(\varepsilon_{\vec{k}} - \varepsilon_{\vec{k'}})$$

$$= f_{imp} \, I_1(\vec{k},\vec{k'})$$

$$I_1(\vec{k},\vec{k'}) = \left| \sum_{\substack{\alpha j \\ \alpha' j}} A^*_{\alpha j} \, A_{\alpha' j'} \sum_{\vec{G},\vec{G}'} \frac{C^j_\alpha(\vec{k}+\vec{G}) \, C^{j'}_{\alpha'}(\vec{k'}+\vec{G}')}{[|\vec{k}+\vec{G}-\vec{k'}-\vec{G}'|^2 + \lambda_0^2]} \right|^2 \frac{\delta_{\varepsilon_{\vec{k}},\varepsilon_{\vec{k'}}}}{|\nabla_{\vec{k'}}\varepsilon_{\vec{k'}}|}$$

where

$$C^j_\alpha(\vec{k}+\vec{G}) = \langle \vec{k}+\vec{G}|\alpha\vec{k}j\rangle$$

$$f_{imp} = 7.965 \times 10^{-5} \, \frac{a \, n_I}{\kappa_\infty^2} \times 10^{12} \quad s^{-1}$$

$$\lambda_0 = 10^{-10} \, \lambda a/\pi$$

where a is the lattice constant in angstroms, n_I is in 10^{20} m^{-3}, and $\hbar$ is Planck's constant divided by 2π. In these expressions, $\vec{k}$ and $\varepsilon_{\vec{k}}$ are in units of $(2\pi/a)$ and eV, respectively.

B. Phonons in Compounds

The potential for scattering from LO phonons in compounds is given by:

$$V_{ep} = i \left[\frac{4\pi e^2 \hbar \omega_l}{2 \, V} \left(\frac{1}{\kappa_\infty} - \frac{1}{\kappa_0} \right) \right]^{1/2} \sum_{\vec{q}} \frac{1}{q} \left(a^\dagger_q \, e^{-i\vec{q}\cdot\vec{r}} - a_q \, e^{i\vec{q}\cdot\vec{r}} \right)$$

where a_q , $a_q^\dagger$ are phonon annihilation and creation operators, ω_l is the longitudinal phonon frequency, V is the crystal volume, and κ_0 is the low-frequency dielectric constant. For a scattering from $\vec{k'}$ to $\vec{k}$,

$$S_{ph}(\vec{k},\vec{k'}) = \begin{cases} N^0_q f_{ph} \, P_1(\vec{k},\vec{k'}) & \text{(absorption)} \\ (N^0_q + 1) f_{ph} \, P_2(\vec{k},\vec{k'}) & \text{(emission)} \end{cases}$$

$$P_1(\vec{k},\vec{k'}) = \left| \sum_{\substack{\alpha j \\ \alpha' j'}} A^*_{\alpha j} \, A_{\alpha' j'} \sum_{\vec{G},\vec{G}'} \frac{C^{j*}_\alpha(\vec{k}+\vec{G}) \, C^{j'}_{\alpha'}(\vec{k'}+\vec{G}')}{|\vec{k}+\vec{G}-\vec{k'}-\vec{G}'|} \right|^2 \frac{\delta_{\varepsilon_{\vec{k}},\varepsilon_{\vec{k'}}-\hbar\omega_l}}{|\nabla_{\vec{k'}}\varepsilon_{\vec{k'}}|_{\vec{k'}}}$$

$$P_2(\vec{k},\vec{k'}) = \left| \sum_{\substack{\alpha j \\ \alpha' j'}} A^*_{\alpha j} \, A_{\alpha' j'} \sum_{\vec{G},\vec{G}'} \frac{C^{j*}_\alpha(\vec{k}+\vec{G}) \, C^{j'}_{\alpha'}(\vec{k'}+\vec{G}')}{|\vec{k}+\vec{G}-\vec{k'}-\vec{G}'|} \right|^2 \frac{\delta_{\varepsilon_{\vec{k}},\varepsilon_{\vec{k'}}+\hbar\omega_l}}{|\nabla_{\vec{k'}}\varepsilon_{\vec{k'}}|_{\vec{k'}}}$$

$$f_{ph} = 86.94 \frac{\hbar\omega_l}{a} \left[\frac{1}{\kappa_\infty} - \frac{1}{\kappa_0}\right] \times 10^{12}$$

$$N_\eta^0 = [\text{Exp}\ (\hbar\omega_l/k_BT) - 1]^{-1}$$

In the calculation of P_1, P_2, and f_{ph} terms, $\vec{k}$ and $\varepsilon_{\vec{k}}$ are in $(2\pi/a)$ and eV, respectively.

C. Intervalley Scattering—Deformation Coupled

While the BZ sum of $I_1(\vec{k},\vec{k}')$, $P_1(\vec{k},\vec{k}')$, $P_2(\vec{k},\vec{k}')$ includes that portion of intervalley scattering mediated by LO phonons and impurities, there is additional intervalley scattering arising from the displacement of atoms from their regular sites. This deformation-potential-coupled intervalley scattering is believed to be very important at high electric fields. However, the strength of this scattering depends sensitively on the less-known deformation potential constant D. We had made an *ab initio* calculation of this D from the underlying band structure (Krishnamurthy, Sher, and Chen, 1988c). Calculated scattering rates successfully explain characteristics of GaAs HET. The scattering rate from $\vec{k}'$ in Γ-valley to $\vec{k}$ in L valley, for example, is given by:

$$S_{iv}(\vec{k},\vec{k}') = \begin{cases} f_{iv}\, P_3(\vec{k},\vec{k}') & \text{(absorption)} \\ f_{iv}\, P_4(\vec{k},\vec{k}') & \text{(emission)} \end{cases}$$

$$P_3(\vec{k},\vec{k}') = \frac{\delta_{\varepsilon_{\vec{k}},\, \varepsilon_{\vec{k}'} + \hbar\omega_0}}{|\nabla_{\vec{k}'}\varepsilon_{\vec{k}'}|_{\vec{k}'}}$$

$$P_4(\vec{k},\vec{k}') = \frac{\delta_{\varepsilon_{\vec{k}},\, \varepsilon_{\vec{k}'} - \hbar\omega_0}}{|\nabla_{\vec{k}'}\varepsilon_{\vec{k}'}|_{\vec{k}'}}$$

$$f_{iv} = 1.332 \times 10^5 \frac{D^2}{a^3\, \rho\, (\hbar\omega_0)} \times 10^{12} \quad s^{-1} \ .$$

All $\vec{k}$ and $\varepsilon_{\vec{k}}$ are in units of $(2\pi/a)$ and eV, respectively. D is in 10^8 eV/cm, a is in angstroms, ρ is in g/cm^3, and $\hbar\omega_0$, the energy phonons necessary for intervalley transfer, is in meV.

D. Alloy Disorder Scattering

The electron transport in alloys, calculated in CPA, is affected by disorder in two ways. The real part of self-energy changes the relationship of ε to k and thus changes the density of states. The imaginary part of self-energy introduces a finite lifetime to these states and thus additional scattering is experienced. In $A_xB_{1-x}C$ alloys, for example, the electron sees different

potential, depending on whether an A or B atom is at that site. If we denote this potential change in site from VCA average in a matrix δV, then the alloy disorder-disorder scattering potential is:

$$\Delta V = \frac{1}{N} \sum_{n} \langle n | \delta V | n \rangle \quad ,$$

where n is the site index and N is total number of sites. Then, for a scattering from $\vec{k}'$ to $\vec{k}$, we have:

$$S_A(\vec{k},\vec{k}') = \frac{2\pi}{\hbar} \; |\langle \vec{k} | \Delta V | \vec{k}' \rangle|^2 \; \delta(\varepsilon_{\vec{k}} - \varepsilon_{\vec{k}'}) \quad ,$$

$$= f_A \; I_2(\vec{k},\vec{k}') \quad ,$$

$$I_2(\vec{k},\vec{k}') = \left| \sum_{\substack{\alpha\alpha' \\ ij'}} A^{*}_{\alpha j} \, A_{\alpha j'} \, \Delta V^{ij'}_{\alpha\alpha'} \right|^2 \frac{\delta_{\varepsilon_{\vec{k}},\, \varepsilon_{\vec{k}'}}}{|\nabla_{\vec{k}} \varepsilon_{\vec{k}'}|} \quad ,$$

$$f_A = 9.48 \times 10^3 \; x(1 - x) \times 10^{12} \quad s^{-1} \quad ,$$

where $\vec{k}$ and $\varepsilon_{\vec{k}}$ are in units of $(2\pi/a)$ and eV, respectively.

E. Phonons in Alloys

In alloys such as $A_xB_{1-x}C$, there will be two kinds of phonons, namely AC-type and BC-type. The coupling constant for interaction with these phonons will be strongly concentration-dependent. Moreover, the number of phonons in each kind will also be concentration-dependent. Hence, polar phonon scattering in alloys can be very different from that in constituent compounds.

The q-dependent dielectric function for phonon-plasmon coupled system is:

$$\varepsilon(q,\omega) = \varepsilon_\infty \left[\frac{\omega^2 - \omega_l^2}{\omega^2 - \omega_t^2} \right] + x(q,\omega) \quad ,$$

where $x(q,\omega)$ in Lindhard form is

$$x(q,\omega) = \chi_1(q,\omega) + i\,\chi_2(q,\omega)$$

$$\chi_1(q,\omega) = \frac{k_{FT}^2}{q^2}\left[\frac{1}{2} + \frac{k_F}{4q}\left\{\left[\left[\frac{\omega + q^2/2m}{qv_F}\right]^2 - 1\right]\ln\left|\frac{\omega - qv_F + q^2/2m}{\omega + qv_F + q^2/2m}\right|\right.\right.$$

$$\left.\left. - \left[\left[\frac{\omega - q^2/2m}{qv_F}\right]^2 - 1\right]\ln\left|\frac{\omega - qv_F - q^2/2m}{\omega + qv_F - q^2/2m}\right|\right\}\right] .$$

When $q < 2k_F$,

$$\chi_2(q,\omega) = \begin{cases} \dfrac{\pi}{2}\dfrac{k_{FT}^2}{q^2}\dfrac{w}{qv_F} & 0 \le \omega \le qv_F - q^2/2m \\ \dfrac{\pi}{4}\dfrac{k_{FT}^2}{q^2}\dfrac{k_F}{q}\left\{1 - \left[\dfrac{\omega - q^2/2m}{qv_F}\right]^2\right\} & -q^2/2m \le \omega - qv_F \le q^2/2m \\ 0 & \omega > q^2/2m + qv_F \end{cases}$$

When $q > 2k_F$,

$$\chi_2(q,\omega) = \begin{cases} \dfrac{\pi}{2}\dfrac{k_{FT}^2}{q^2}\dfrac{k_F}{q}\left[1 - \left[\dfrac{\omega - q^2/2m}{qv_F}\right]^2\right] & q^2/2m - qv_F \le \omega \le q^2/2m + qv_F \\ 0 & \text{otherwise} \end{cases}$$

with

$$k_{FT}^2 = \frac{6\pi ne^2}{\varepsilon_F} \quad \text{(Thomas–Fermi screening)}$$

$$V_{ep} = i\left[\frac{4\pi e^2\hbar}{\kappa_\infty V}\right]^{1/2}\sum_q \frac{1}{q}\left[\frac{\Delta_1}{\omega_{11}^2}\left[1 + \frac{\Delta_2^2}{\Delta_{12}^2}\right]^{1/2}(a_{1q}\,e^{i\vec{q}\cdot\vec{r}} - a_{1q}^\dagger\,e^{-i\vec{q}\cdot\vec{r}})\right.$$

$$\left. + \frac{\Delta_2}{\omega_{12}^2}\left[1 - \frac{\Delta_1^2}{\Delta_{12}^2}\right](a_{2q}\,e^{iq\cdot r} - a_{2q}^\dagger\,e^{-iq\cdot r})\right]$$

$$S(\vec{k},\vec{k}') = 10^{12} \times 86.94 \left[(1-x) \frac{\hbar\omega_{l1}}{\kappa_\infty a} \frac{\Delta_1^2}{\omega_{l1}^2} \left[1 + \frac{\Delta_2^2}{\Delta_{12}^2} \right] \right.$$

$$\times \left\{ N_{q_1} P_1(\vec{k},\vec{k}';\hbar\omega_{l1}) + (N_{q_1} + 1) P_2(\vec{k},\vec{k}';\hbar\omega_{l1}) \right\}$$

$$\left. + \frac{\hbar\omega_{l2}}{\kappa_\infty a} \frac{\Delta_2^2}{\omega_{l2}^2} \left[1 - \frac{\Delta_2^2}{\Delta_{12}^2} \right] \left\{ N_{q_2} P_1(\vec{k},\vec{k}';\hbar\omega_{l2}) + (N_{q_2} + 1) P_2(\vec{k},\vec{k}';\hbar\omega_{l2}) \right\} \right]$$

$$\Delta_1^2 = \omega_{l1}^2 - \omega_{t1}^2$$

$$\Delta_2^2 = \omega_{l2}^2 - \omega_{t2}^2$$

$$\Delta_{12}^2 = \omega_{l1}^2 - \omega_{l2}^2 \quad ,$$

where $\hbar\omega_{l1}$ ($\hbar\omega_{t1}$) is LO (TO) phonon energy in the case of x = 0 and $\hbar\omega_{l2}$ ($\hbar\omega_{t2}$) in the case of x = 1; $\hbar\omega_{li}$ is in meV, a is in angstroms, and $\vec{k},\vec{k}'$ are in units of (2π/a). m is electron mass and n is the electron density. The functions P_1 , P_2 , and N_q are defined in Section II-B. k_F , v_F, and ε_F are Fermi wave vector, velocity, and energy, respectively.

F. Electron-Electron Scattering

It is believed that in a heavily doped semiconductor electron-electron scattering represents the fundamental limitation on the electron mean free path. To quantify this effect, we have calculated the velocity relaxation time in effective mass approximation as follows. For the scattering $\vec{k}$ to $\vec{k}'$,

$$S(\vec{k},\vec{k}') = -8\pi\, e^2 \int d\omega\, \mathrm{Im}\left[\frac{1}{\varepsilon(q,\omega)} \right] \delta(\varepsilon_{\vec{k}'} - \varepsilon_{\vec{k}\pm\vec{q}} \pm \hbar\omega)$$

where $\vec{k}'$ is $\vec{k} \pm \vec{q}$ and the $\pm$ denotes the absorption or emission process.

III MATERIALS CHOICES FOR BALLISTIC MODE DEVICES: HOT ELECTRON TRANSISTORS

Both GaAs and InAs, two important materials, are direct-gap materials; the central-valley Γ-minimum is the bottom of the conduction band, the L-valley minimum in the (111) direction is next lowest, and the X-valley in the (100) direction is higher still. The group velocity $V_g(k)$ at any wave vector k is given in terms of the band energies $\varepsilon(k)$ by

$$V_g(\vec{k}) = \frac{1}{\hbar}\nabla\varepsilon(\vec{k}) \quad .$$

We have shown (Krishnamurthy, Sher, and Chen, 1988a, 1988b) that, for the direct-gap materials, the group velocity reaches its highest values for electrons injected in the (100) direction. Thus, the remaining discussion is confined to injection in the (100) direction. Figure 1 shows the group velocity as a function of injected energy for several semiconductors. The peak in v_g for GaAs is $v_{gp} \simeq 1.2 \times 10^8$ cm/s and at E ≈ 0.8 eV; however, the curve is quite flat over an extended range of energies. Only InAs and the $Ga_{1-x}In_xAs$ alloys have a v_{gp} larger than that of GaAs. However, because the band gap of InAs is small, electrons injected at energies near its v_{gp} can cause a breakdown. The bandgap of the $Ga_{0.5}In_{0.5}As$ alloy is large enough to preclude this problem.

Clearly the optimum strategy to maximize device speed is to inject the electrons from the source at their peak group velocity, $\vec{v}_{gp}$. If this is done, any attempt to accelerate them with applied fields is useless, because any change in k will decrease their velocity. There is another concern, however. If the scattering rate at v_{gp} is high enough that the velocity mean free path is low, and if few electrons reach the drain, the device efficiency will be low. Thus, a compromise between speed and efficiency may be required. The velocity mean free path is

$$\lambda_v(\vec{k}) = v_g(\vec{k})\tau_v(\vec{k}) \quad ,$$

where $\tau_v(k)$ is the velocity collision time for the injected electrons. The velocity relaxation time reduces to the momentum relaxation time only in the special case of the constant effective mass, which is far removed from the situation here. Figure 2 shows the velocity mean free path for several semiconductors as a function of energy for electrons traveling in the (100) direction. Once again, the $Ga_{0.5}In_{0.5}As$ alloy is the only practical material with a Λ_v greater than that of GaAs (Krishnamurthy, Sher, and Chen, 1988a, 1988b). These calculations include all scattering mechanisms except the deformation-potential-coupled phonon interaction. The donor concentration is taken to be 10^{18} cm^{-3}. The Γ to L and X energy separations in GaAs are 0.3 eV and 0.55 eV, respectively. Nothing dramatic happens to the GaAs curve (c) at these energies, because the intervalley scattering entails a large momentum transfer, and the longitudinal optical phonon and impurity matrix elements decrease as $1/\Delta k$ and $1/\Delta k^2$, respectively. This is because these interactions are long range; hence, their Fourier components in momentum space reach a peak at low Δk. While the deformation potential coupling constant

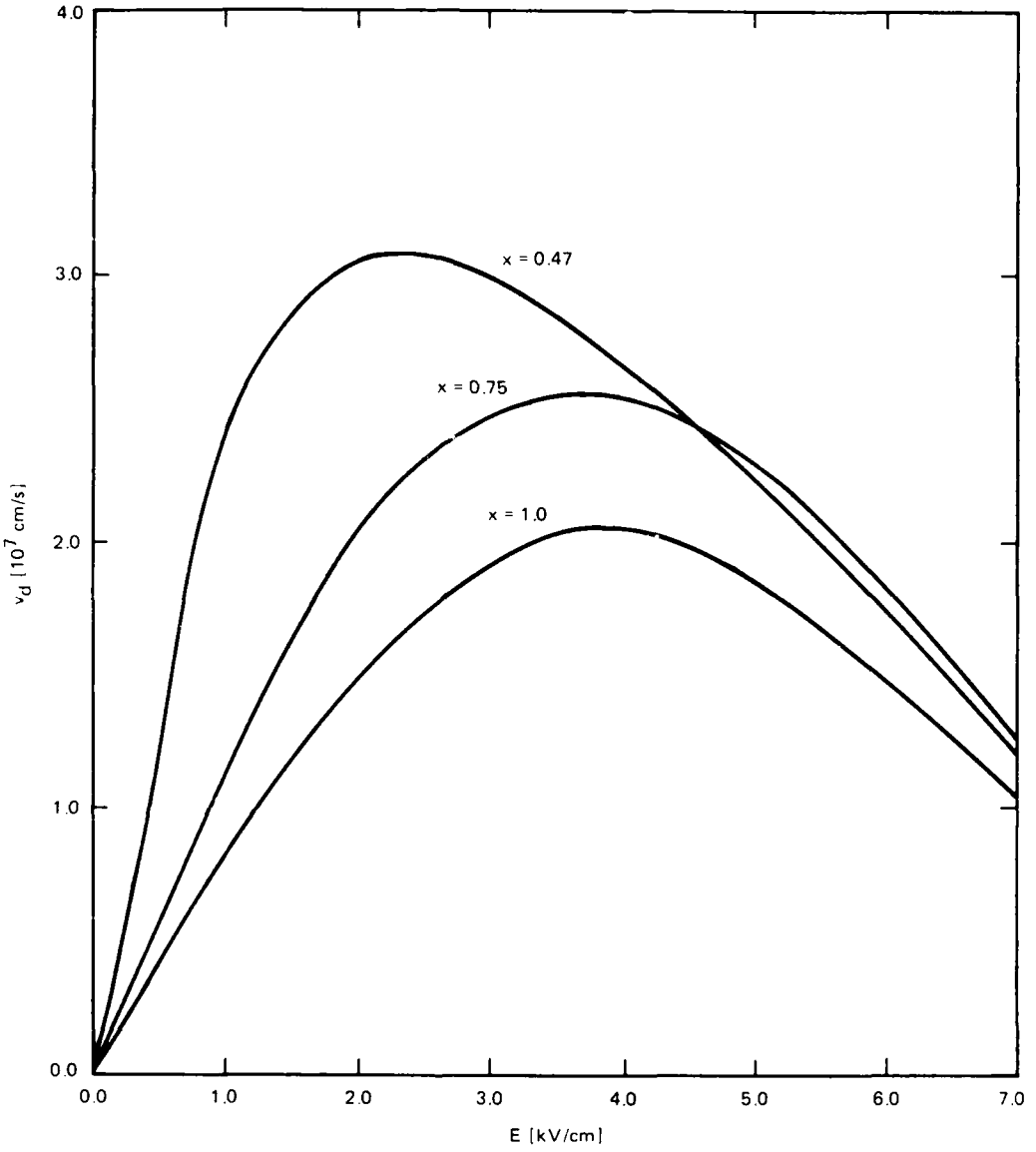

FIGURE 1 VELOCITY-FIELD CHARACTERISTICS OF GaAs-BASED ALLOYS

for low Δk is far smaller than that of the polar optical coupling constant, it does not fall for high Δk because it is a short-range interaction. Thus, while the deformation potential contributes little to intravalley scattering, it is important in intervalley scattering.

We have calculated the deformation potential for intervalley coupling constant for GaAs from the underlying band structure (Krishnamurthy, Sher, and Chen, 1988c). We find $D = 3.25 \times 10^8$ eV/cm, compared to the generally accepted value 5.1×10^8 eV/cm. Because D^2

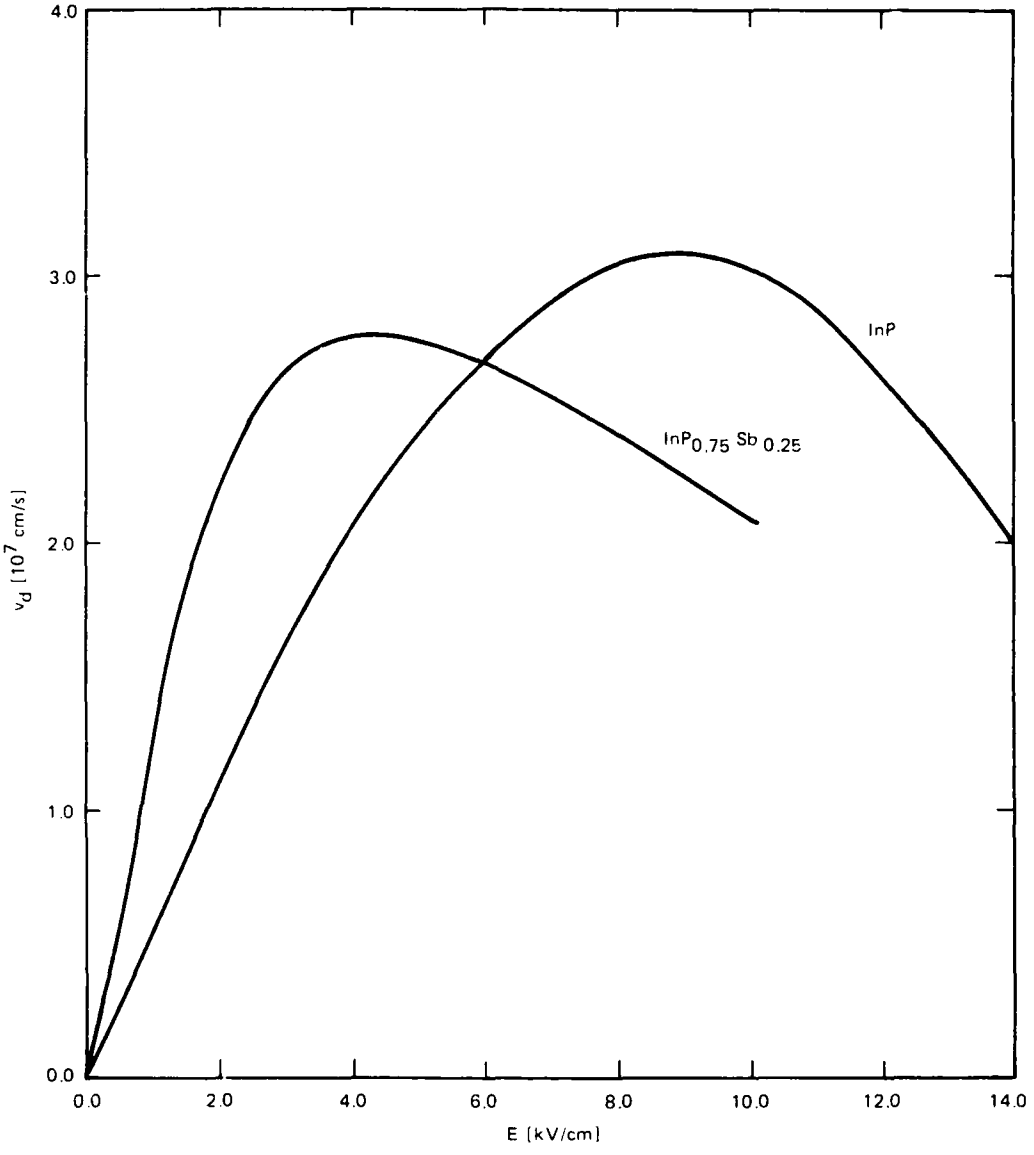

FIGURE 2 VELOCITY-FIELD CHARACTERISTICS OF InP-BASED ALLOYS

enters into the scattering range, this is a large difference. However, as discussed in the introduction, when placed in a full band structure calculation (where the density of states is higher than found in the effective-mass approximation), the net scattering rates with the smaller D and proper density of states and the larger D but small density of states are not too different. We have calculated the injection energy variation of α, the ratio of the drain to source current for

the HET structure. Our prediction agrees closely with experiment (Krishnamurthy, Sher, and Chen, 1988c). This theory has no adjustable parameters. We conclude that, for the geometry used, the experiment actually reached an ideal limiting result for a GaAs HET.

We have calculated the upper cut-off frequency and α for a number of materials that are given in Table 1. The calculations do not include deformation-potential scattering; hence, the reported results are for conditions in which the injection energy is below the Γ-L valley separation. Thus, there is no intervalley scattering. For the thicker (500-Å) devices, InAs and $Ga_{0.5}In_{0.5}As$ are better than GaAs. (These InAs numbers were found for an injection energy below the bandgap energy to avoid breakdown.) However, for very thin devices, GaAs is as good as any other material considered here and is the simplest material to fabricate. Notice that $Ga_{0.7}Al_{0.3}As$ is substantially poorer than the others, and one should avoid its use in the active regions of the devices. We have examined all the other semiconductors and none are better than the materials in Table 1 (Krishnamurthy, Sher, and Chen, 1988a, 1988b).

Table 1

CUTOFF FREQUENCY v_c AND FRACTION OF INJECTED ELECTRONS α_{bal} FOR TWO BASE WIDTHS

	Base Width = 500 Å		Base Width = 100 Å	
Alloy	v_c (THz)	α_{bal}	v_c (THz)	α_{bal}
GaAs	3.1	0.63	15.6	0.91
$Ga_{0.5}In_{0.5}As$	4.1	0.82	20.7	0.96
InAs	4.3	0.86	21.5	0.97
$InAs_{0.5}P_{0.5}$	4.1	0.76	20.7	0.95
InP	3.7	0.64	18.6	0.91
$Ga_{0.7}Al_{0.3}As$	1.7	0.04	8.3	0.54

IV MATERIALS CHOICES FOR DRIFT-TRANSPORT-MODE DEVICES

A. Electron-Temperature Model

The electron drift velocity v in many semiconductors increases linearly under the influence of electric field to reach a peak value v_p at a threshold field, E_T; any further increase in E results in reduced v, giving rise to a negative differential resistance. High-speed device applications benefit from materials with maximum v_p and minimum E_T.

The v-E curves are calculated in a variety of approximations. In the simplest (two-valley) model, each valley is characterized by a different effective mass. Their minima are separated by an offset energy ΔE; these three parameters, together with the electron-phonon coupling constant, are adjusted to fit the observed v-E curves. Various authors have evaluated the effect of disorder scattering on low field mobility in the alloys. The main difficulty in extending these models to the hot electron problem is in applying the appropriate correction to the change in the effective mass and scattering potential with wave vector $\vec{k}$. Our improvement over previous efforts is to use realistic and accurate band structures in evaluating various scattering rates and parameters needed to obtain v-E curves (Krishnamurthy, Sher, and Chen, 1987). In the alloys, CPA band structure is used where the alloy scattering obtained directly from the imaginary part of the CPA self-energy. In this formalism, the nonparabolic, anisotropic and intervalley scattering mediated by alloy disorder are included without adjustable parameters.

In this electron-temperature model, the electrons are assigned a temperature T_e, which is usually much higher than lattice temperature T. This is because the average electron energy under high electric field is much larger than the average lattice excitation energy per particle. If we denote the mobility in the lower valley as μ_1 and assume that the mobility in the higher valley is zero, then:

$$v = \mu_1 E \left[1 + R\, e^{-\frac{\Delta E}{k_B T_e}} \right]^{-1} , \tag{4-1}$$

where R is the ratio of density of states in the upper valley to that of lower valley. In the steady state, the energy gained by an electron from the field must be balanced by the energy lost to the lattice:

$$evE = \frac{3}{2} k_B \frac{(T_e - T)}{\tau_E} , \tag{4-2}$$

where τ_E is the energy relaxation time. Equations (4-1) and (4-2) can be combined to yield T_e and v-E characteristics. In the case of alloys, the concentration dependence of R, ΔE and μ_1 are used to obtain v-E curves. The results of these calculations have been published

(Krishnamurthy, Sher, and Chen, 1987). We concluded that $Ga_{0.47}In_{0.53}As$ alloys and InP-based alloys such as $InP_{0.75}As_{0.25}$ and $InP_{0.75}Sb_{0.25}$ are preferable to GaAs for high-speed device applications.

B. Solution to the Boltzmann Equation: An Eigenvalue Method

Although the full band structure is used in the calculations described in Section IV-A, the results offer only qualitative trends. This is because of various approximations such as electron temperature, displaced Maxwellian and energy relaxations, and the like. To obtain quantitatively accurate results, one must solve Boltzmann transport (BT) equation without such limiting approximations. Techniques such as Monte Carlo combined with the Rees algorithm are widely used to obtain the distribution function by solving semiclassical BT equation. The numerical computation is tedious and time-consuming; generalization of this method to include full band structure is computationally more time-consuming. To circumvent this problem, we developed an eigenvalue method to solve the steady-state BT equation. This method of obtaining solution is about two to three orders of magnitude faster than the existing methods (Krishnamurthy, Sher, and Chen, 1988d).

We here describe this method in brief. The steady state BT equation is

$$\frac{eE}{\hbar}\frac{df(\vec{k})}{dk_z} - \sum_{\vec{k}'}[S(\vec{k},\vec{k}')\, f(\vec{k}) - f(\vec{k}',\vec{k})\, f(\vec{k})] = 0 \quad . \tag{4-3}$$

E is assumed to be in $\hat{z}$ direction. If we expand the distribution function, $f(\vec{k})$, in terms of a complete set, $\{\phi_i(\vec{k})\}$, then

$$f(\vec{k}) = \sum_i \phi_i(\vec{k})\, C_i \quad . \tag{4-4}$$

Substituting Eq. (4-3) in Eq. (4-2), we get a matrix equation,

$$\mathbf{MC} = \mathbf{0} \tag{4-5}$$

where **M** is a $(n \times n)$ matrix , **C** is a column matrix, and **0** is a null column matrix; n is the number of basis functions in the chosen basis set. From Eq. (4-5), we see that the eigenvector corresponding to zero eigenvalue of the **M** gives us the expansion coefficients necessary to obtain the distribution function, as given in Eq. (4-4).

If the chosen basis set is complete, the eigenvalue zero is ensured and the distribution function can be accurately obtained. However, if the basis set contains very large number of functions, then a numerically difficult diagonalization of very large matrix must be carried out. Hence, we need to make an educated guess of the basis set that is finite and that can accurately describe the distribution function in high electric fields. In all calculations reported here, we assumed two basis function (s and p_z-like) at each Γ, L, and X valleys. The applied electric field is assumed to be in Z direction. Because L valleys are symmetrically located with respect

to field direction, the number of basis functions in L valleys can reduced to just two. However, we need two set of basis function at X valleys (one set at the X valley in the $\vec{E}$ direction and the other set at X valley perpendicular to the $\vec{E}$ direction). Hence, we have eight basis function in our basis set, given as follows:

$$\phi_1 = N_1 \, e^{-\alpha_1 \varepsilon_{\vec{k}}} \tag{4-6}$$

$$\phi_2 = N_2 \, \frac{d\varepsilon_{\vec{k}}}{dk_z} \, e^{-\alpha_2 \varepsilon_{\vec{k}}}$$

$$\phi_3 = N_3 \, e^{-\beta_1(\varepsilon_{\vec{k}} - \varepsilon_L)}$$

$$\phi_4 = N_4 \, \frac{d\varepsilon_{\vec{k}}}{dk_z} \, e^{-\beta_2(\varepsilon_{\vec{k}} - \varepsilon_L)}$$

$$\phi_5 = N_5 \, e^{-\gamma_1(\varepsilon_{\vec{k}} - \varepsilon_x)}$$

$$\phi_6 = N_6 \, e^{-\gamma_1(\varepsilon_{\vec{k}} - \varepsilon_x)} \, \frac{d\varepsilon_{\vec{k}}}{dk_z}$$

$$\phi_7 = N_7 \, e^{-\gamma_1(\varepsilon_{\vec{k}} - \varepsilon_y)}$$

$$\phi_8 = N_8 \, e^{-\gamma_1(\varepsilon_{\vec{k}} - \varepsilon_y)} \, \frac{d\varepsilon_z}{dk_z}$$

where N_i are the normalization constants. Owing to the finiteness of the basis set, the zero eigenvalue of **M** is not ensured. As a tradeoff for a large basis set, we introduced an iterative procedure. In all calculations reported here, we set $\alpha_i = \beta_i = \gamma_i = \alpha$. We varied α to obtain the zero eigenvalue. In most cases, the zero eigenvalue is obtained in less than 10 iterations where each iterations takes approximately 2 Cray CPU seconds. Once the eigenvectors that correspond to zero eigenvalue are obtained, the distribution is calculated from Eq. (4-4). The drift velocity can then be calculated from

$$v_d = \frac{1}{N} \sum_{\vec{k}} v_z(\vec{k}) \, f(\vec{k}) \tag{4-7}$$

where $v_z = d\varepsilon_{\vec{k}}/dk_z$.

Figures 1 and 2 show, respectively, calculated v-E curves for GaAs-based alloys and InP-based alloys. Comparative evaluation is made in Figure 3. In the lower panel of Figure 3, E_p the minimum energy necessary for pair production and ΔE is plotted for various alloys and compounds. Those alloys in which $\Delta E < E_p$ cannot be used efficiently for high-speed device applications as the breakdown is expected before reaching the peak velocity. The upper panel of Figure 3 shows $\tilde{v}_p$ and $\tilde{E}_T^{-1}$ for various alloys and compounds. $\tilde{v}_p$ and $\tilde{E}_T^{-1}$ are the ratio of

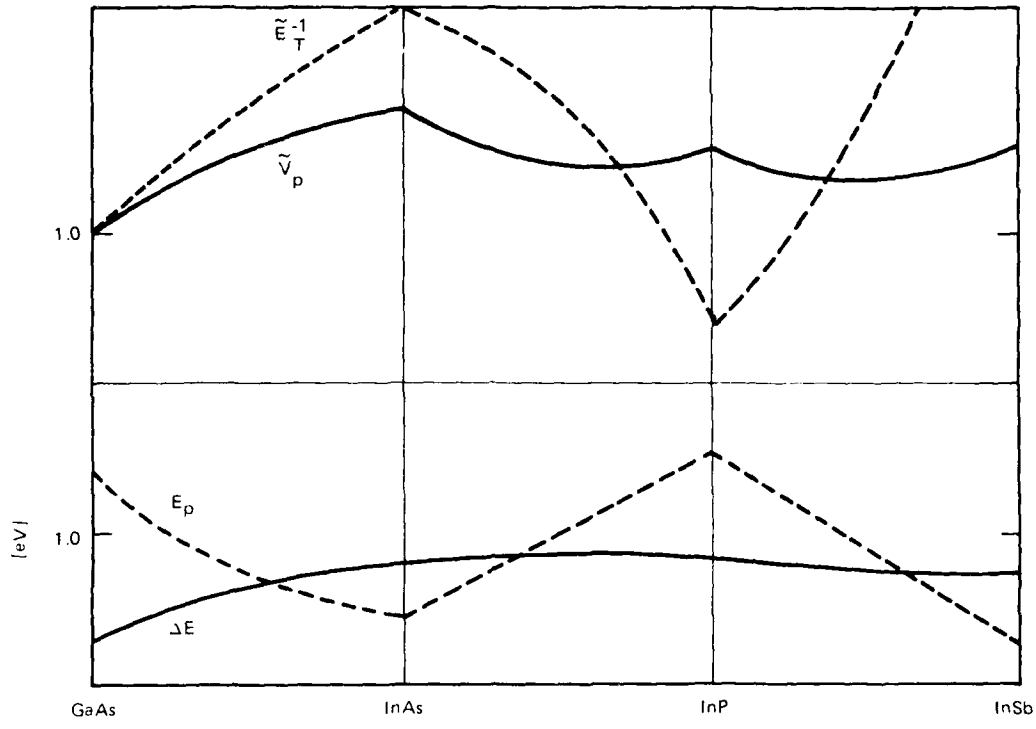

FIGURE 3 COMPARATIVE EVALUATION OF VARIOUS SEMICONDUCTOR ALLOYS FOR HIGH-SPEED DEVICE APPLICATIONS

peak velocity and threshold field in the material to that in GaAs. The materials in which $\tilde{v}_p$ and $\tilde{E}_T^{-1}$ are larger than unity, are preferable to GaAs for high-speed and power device applications. Our calculations suggest that $Ga_{0.47}In_{0.53}As$, $InP_{0.75}Sb_{0.25}$, and $InP_{0.75}Sb_{0.25}$ are superior to GaAs.

V HIGHLIGHTS AND CONCLUSIONS

An accurate transport calculation for ballistic and drift mode devices is reported here. The incorporation of this transport theory into device modeling codes should make it possible to develop a computer-aided design model for these structures. Thus, we are one step closer to materials engineering to a purpose.

Based on this 36-month study of hot electron transport in semiconductors and alloys, we conclude the following:

(1) The v-E curves obtained in the EMA are quantitatively different from that obtained by using full band structures (Krishnamurthy, Sher, and Chen, 1987).

(2) Alloy scattering is important and affects the v-E curves substantially. Because this scattering increases with density of states, it becomes very important in high field transport (Krishnamurthy, Sher, and Chen, 1987).

(3) The strength of alloy scattering depends sensitively on the scattering potential used. In CPA formalism adapted here, the scattering potential emerges naturally from the underlying band structure (Krishnamurthy, Sher, and Chen, 1987; Krishnamurthy, Sher, and Chen, 1988).

(4) Results using electron temperature two-valley model depend sensitively on the energy relaxation time.

(5) Velocity relaxation rate and velocity mean free path are the appropriate quantities to study the hot-electron transistor characteristics (Krishnamurthy, Sher, and Chen, 1988a; 1988b).

(6) The fraction of electrons that are ballistic in ballistic devices depend strongly on electron electron scattering. However, the ratio of collector current to emitter current, α, is affected by electron-electron scattering only by 10% even in $10^{18}cm^{-3}$ (Krishnamurthy, Sher, and Chen, 1988c).

(7) The coupling constant for deformation potential coupled intervalley scattering is calculated from the underlying band structure. The calculated strength of the intervalley scattering explains the measured α in GaAs hot electron transistor (HET) very well (Krishnamurthy, Sher, and Chen, 1988c). The calculated coupling constant is much smaller than the ones currently used in the literature. Because the measured α agrees with our calculated one, it demonstrates that a near-ideal HET was made and no further increase in its function should be expected.

(8) Owing to the changing curvature of the band structure, the obtained velocity scattering rates for impurities and phonons are larger than that obtained in EMA.

(9) For ballistic transport devices with thicker width (approximately 500 Å), InAs and $Ga_{0.5}In_{0.5}As$ materials are expected to be more efficient than GaAs (Krishnamurthy, Sher, and Chen, 1988a; 1988b).

(10) For ballistic devices with very thin base width (approximately 100 Å), no material offers greater advantages than GaAs (Krishnamurthy, Sher, and Chen, 1988a; 1988b).

(11) We had developed a new and faster numerical method to solve the steady-state Boltzmann transport (BT) equation. This iterative solution to BT equation can be obtained in typically 2 cpu seconds on the CRAY-2 (Krishnamurthy, Sher, and Chen, 1988d).

(12) Using only eight basis functions, we have obtained v-E curves up to 15 kV/cm of electric field. The calculated peak velocity and threshold field are in excellent agreement with experiments. It should be pointed out that these results are obtained with absolutely no adjustable parameter.

(13) Our calculations suggest that $Ga_{0.47}In_{0.53}As$, $InP_{0.75}As_{0.25}As$ and $InP_{0.75}Sb_{0.25}As$ are better than GaAs for high-speed device applications. $Ga_{0.47}In_{0.53}As$ is the most efficient of all the candidates considered here for these applications (Krishnamurthy, Sher, and Chen, 1988d).

(14) To obtain solution to BT equation at higher electric fields, the number of basis functions must be increased to describe the distribution function adequately. This improvement should be carried out to obtain peak-to-valley ratio and saturation drift velocity in these alloys.

(15) This eigenvalue method should be slightly modified for the cases of spatially varying electric field.

REFERENCES

Krishnamurthy, S., A. Sher, and A.-B. Chen, 1986: "Band Structure of Si_xGe_{1-x} Alloys," *Phys. Rev. B*, Vol. 33, p. 1026.

Krishnamurthy, S., A. Sher, and A.-B. Chen, 1987: "Velocity-Field Characteristics of III-V Semiconductor Alloys: Band Structure Influences," *J. Appl. Phys.*, Vol. 61, p. 1475.

Krishnamurthy, S., A. Sher, and A.-B. Chen, 1988a: "Materials Choice for Ballistic Transport: Group Velocities and Mean-Free Paths Calculated from Realistic Band Structures," *Appl. Phys. Lett.*, Vol. 52, p. 468.

Krishnamurthy, S., A. Sher, and A.-B. Chen, 1988b: "Ballistic Transport in Semiconductor Alloys," *J. Appl. Phys.*, Vol. 63, p. 4540.

Krishnamurthy, S., A. Sher, and A.-B. Chen, 1988c: "Deformation Potential and Intervalley Scattering: Hot Electron Transistor Analysis," *Appl. Phys. Lett.*, (in press).

Krishnamurthy, S., A. Sher, and A.-B. Chen, 1988d: "Solution to Boltzmann Equation: An Eigen Value Method," *Phys. Rev. B* (in preparation).

PUBLICATIONS AND CONFERENCE PAPERS PREPARED UNDER THIS CONTRACT

Below is the summary of all written and oral output connected with this research.

Journal Publications

"Generalized Brooks Formula and Electron Mobility in Si_xGe_{1-x} Alloys," *Appl. Phys. Lett.*, Vol. 47, No.2, p.160 (1985).

"Band Structure of Si_xGe_{1-x} Alloys," *Phys. Rev. B*, Vol. 33, p. 1026 (1986).

"Velocity-Field Characteristics of III-V Semiconductor Alloys: Band Structure Influences," *J. Appl. Phys.*, Vol. 62, No.4, p. 1475 (1987).

"Alloy Electronic Structure Statistics," Seventh International Conference on Ternary and Multinary Compounds, p. 377 (1987).

"Structure-Property Relationships in Semiconductor Alloys," *Mat. Res. Soc. Symp.*, Vol. 90, p. 91 (1987).

"Semiconductor Alloys for High Speed Device Electronics," First International SAMPE Electronics Conference, p. 318 (1987).

"Electronic and Transport Properties of HgCdTe and HgZnTe," *J. Vac. Sci. Technol.*, A5, p. 3014 (1987).

"Material Choice for Ballistic Transport: Group Velocities and Mean Free Path Calculated from Realistic Bandstructures," *Appl. Phys. Lett.*, Vol. 52, No. 6, p. 468 (1988).

"Ballistic Transport in II-VI Semiconductor Compounds and Alloys," *J. Cryst. Growth*, Vol. 86, p. 33 (1988).

"Systematics of Chemical and Structural Disorder on Band Edge Properties of Semiconductor Alloys," *Phys. Rev. B*, Vol. 37, p. 4254 (1988).

"Ballistic Transport in Semiconductor Alloys," *J. Appl. Phys.*, Vol. 63, No. 9, p. 4540 (1988).

"Semiconductor Alloys for Fast Thermal Sensors," *J. Appl. Phys.*, Vol. 64, No. 3, p. 1530 (1988).

"Deformation Potential and Intervalley Scattering: Hot Electron Transistor Analysis," *Appl. Phys. Lett.*, (1988) (in press).

"Solution to Boltzmann Equation: An Eigen Value Method," *Phys. Rev. B*, (in preparation) (1988).

"Transport in Submicron Devices," Proceedings of 14th International Conference on Microlithography and Microcircuit Engineering (Vienna,Austria), September 20-22, 1988.

Contributed Conference Papers

"Calculation of Band Edge Properties in Semiconductor Alloys," March Meeting of the American Physical Society (1986).

"Electronic Properties of HgZnTe," March Meeting of the American Physical Society (1986).

"Preliminary CPA Velocity Field Curves of Semiconductor Alloys," March Meeting of the American Physical Society (1986).

"Material Engineering for Drift Devices," EHF Monolithic Materials and Devices, DARPA Joint Contractor Review (1986).

"Hot Electron Transport in Semiconductor Alloys," March Meeting of the American Physical Society (1987).

"Material Engineering for Ballistic and Drift Devices," EHF Monolithic Materials and Devices, DARPA Joint Contractor Review (1987).

"Semiconductor Alloys for High Speed Device Electronics," First International SAMPE Electronics Conference, Santa Clara Monolithic Materials and Devices, DARPA Joint Contractor Review (1988).

"Intervalley Scattering in Semiconductors," March Meeting of the American Physical Society (1988).

"Semiconductor Alloys for Fast Thermal Sensors," March Meeting of the American Physical Society (1988).

"Transport in Submicron Devices," 14th International Conference on Microlithography and Microcircuit Engineering, Vienna, Austria, September 20-22, 1988.